

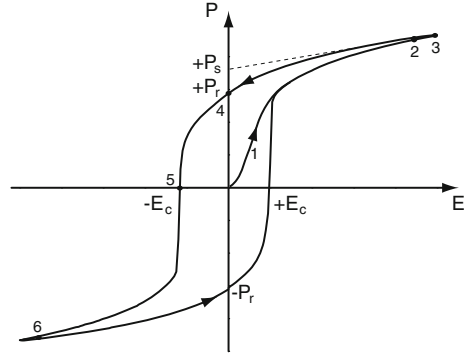
Chapter 2

Domain Walls in Ferroelectric Materials

2.1 General Properties of Ferroelectrics

Ferroelectric materials are characterized by a finite electric polarization in absence of an external electric field. Furthermore, this polarization must possess at least two stable states, and must have the ability to be reversibly switched from one state to another by the application of an electric field. Thus, regions with different orientations of the polarization vector may coexist within a ferroelectric sample, and are called *ferroelectric domains*. Experimentally, the ability to switch from one state to another can be observed by an indirect measurement of the polarization as a function of an applied electric field, and takes the form of a signature *hysteresis loop*, as illustrated in Fig. 2.1. Starting at the origin ($P = 0$, $E = 0$, possible macroscopically if the sample has multiple domains compensating each other) and ramping up the field (1), the total polarization gradually increases towards a saturation value (2) corresponding to all unit cells coherently oriented with the field. Upon further increasing the field, the polarization is further enhanced by dielectric charging (3). When the field is decreased back to zero, the total polarization decreases a little but remains finite, and the polarization value reached at $E = 0$ is called the remanent polarization $+P_r$. When the field is increased in the opposite direction, the polarization state switches suddenly for a specific field intensity called the coercive field $-E_c$. Upon further increase, the polarization saturates and a simple dielectric response is reached again (6). Generally, the same behavior is observed when the electric field is reversed, and repeated cycling results in a symmetric *hysteresis loop*, with switching events at $\pm E_c$. In the presence of internal fields, e.g. due to charge accumulation in a ferroelectric transistor, the hysteresis loop may however be offset with respect to $E = 0$, a phenomenon known as *imprint*. The spontaneous polarization $\pm P_s$ is usually defined as the extrapolation at zero field of the polarization value at high fields, where the slight decrease is due to charging. Ideally, P_r and P_s should be identical. In reality, P_s is often higher in polycrystalline materials (due for instance to the formation of opposite domains during the ramping of the field to zero), but can be very close in single crystals [1].

Fig. 2.1 Ideal hysteretic behavior of the ferroelectric polarization in an applied electric field, considered at a macroscopic scale. For detailed description, see text. Original picture by Dr. N. Stucki



At high temperatures, most ferroelectric materials exist in a paraelectric, generally centrosymmetric phase, and exhibit a simple dielectric response to applied electric fields. As they are cooled down below a critical temperature, called the Curie temperature T_C , they undergo a structural phase transition to a lower crystal symmetry phase, which allows the appearance of the spontaneous polarization.¹ Among the 32 crystallographic point groups, which classify crystal structures based on their symmetry, 21 are noncentrosymmetric, a necessary criterion to fulfill the above requirements. In 20 of these 21 groups,² this lack of inversion symmetry is at the origin of *piezoelectricity*, the appearance of an electric polarization as a consequence of mechanical stress. The *piezoelectric effect* is a linear coupling between the polarization and the stress field:

$$P_i = d_{ijk}\sigma_{ijk}, \quad (2.1)$$

where P is the polarization vector, d the piezoelectric tensor and σ the stress tensor. The piezoelectric tensor is specific to the material, with the nonzero elements dependent on the crystal symmetry, thus restricting the possible polarization vector directions. By energy conservation, the same tensor also describes the *inverse piezoelectric effect*, coupling the strain of the material to an external electric field:

$$\epsilon_{ij} = E_k d_{kij}, \quad (2.2)$$

where ϵ is the strain tensor and E the electric field vector. Both effects can be visualized in Fig. 2.2.

Among the 20 piezoelectric crystal point groups, 10 possess a single polar axis, and are therefore characterized by *pyroelectricity*, i.e. the temperature dependence of the electric polarization. In simple pyroelectric materials, the direction of the

¹ Some ferroelectric materials rather undergo a ferroelectric phase transition from a microscopically polar but macroscopically nonpolar high temperature phase (so-called order-disorder phase transition), and in some cases the phase transition can exhibit both characters together.

² The cubic group 432, although noncentrosymmetric, has other symmetry elements that exclude piezoelectricity.

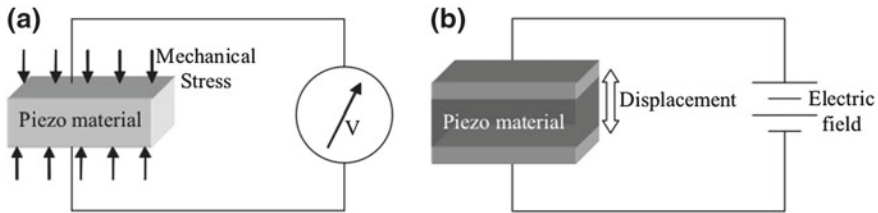


Fig. 2.2 *Left piezoelectric effect.* An electric potential is generated within the material under an applied mechanical stress. *Right inverse piezoelectric effect.* Mechanical deformations are induced under an applied electric field. Figures reproduced from [2]

polarization vector is fixed by the crystal structure, and only its magnitude can be changed by an applied electric field. Thus, ferroelectric materials possess the qualities of piezoelectric and pyroelectric materials, but must in addition exhibit the property of a reversibly orientable polarization vector between at least two ground states. Historically speaking, the pyroelectric properties of some materials, in particular tourmaline, were already known in Antiquity, due to the surface charge redistribution upon heating allowing them to attract small objects. The phenomenon was however not named and quantitatively studied until 1824 by D. Brewster [3]. Piezoelectricity and ferroelectricity were only discovered in 1880 and 1920, by J. and P. Curie [4] and J. Valasek [5] respectively.

Originally, the term “ferroelectricity” was coined in analogy with the similar behavior of ferromagnets, which possess a finite switchable magnetization, such as that of iron (“ferro”), the canonical ferromagnetic metal. However, this similarity is only manifest from a purely macroscopic, thermodynamic point of view, as the microscopic mechanisms that give rise to a spontaneous electric or magnetic polarization are radically different. It is therefore remarkable that the general macroscopic properties of both orders may be commonly described in a statistical approach, relying exclusively on symmetry considerations and neglecting the microscopic details of the system. More broadly, the term “ferroic” can be used to encompass all materials possessing a spontaneous order parameter switchable under an applied conjugate field.

2.2 Thermodynamic Description of Ferroic Materials

In a very general, purely statistical approach, a ferroic material can be defined as system which undergoes a thermodynamic phase transition upon cooling towards a lower symmetry phase, with the appearance of an order parameter with at least two equivalent energy states. For the definition to be complete, this order parameter must be reversibly switchable between the different possible states by the application of an external field.

Following this definition, a very natural way to describe ferroic materials is provided by the thermodynamic formalism of Landau-Ginzburg-Devonshire (LGD) theory of phase transitions, which relies on the concept of broken symmetry. In a nutshell, the theory predicts the sudden disappearance, below a critical temperature T_0 , of a certain symmetry element, leading to a lower symmetry ordered phase. This transition is marked by the value of a certain order parameter ψ , which is zero in the high symmetry phase and different from zero in the ordered phase.³ LGD theory is based on the assumption that, in the vicinity of the phase transition where ψ becomes arbitrarily small, the free energy of the system F can be expanded in a power series of ψ , where only those terms compatible with the symmetry of the system are included⁴:

$$F = F_0 + \sum_n \frac{1}{n} \alpha_n \psi^n, \quad (2.3)$$

where F_0 is the free energy of the high symmetry phase and unrelated to the phase transition, and the α_i coefficients are parameters of the system [6].

The stability condition requires that $F(\psi)$ be a minimum for the equilibrium value of ψ :

$$\left(\frac{\partial F}{\partial \psi} \right) \Big|_{\psi_{equ}} = 0, \quad \left(\frac{\partial^2 F}{\partial \psi^2} \right) \Big|_{\psi_{equ}} > 0. \quad (2.4)$$

For $T > T_0$, the equilibrium value is $\psi = 0$ so that $\alpha_1 = 0$ and $\alpha_2 > 0$; for $T < T_0$, ψ takes a nonzero value so that $\alpha_2 < 0$. Therefore, $\alpha_2 = 0$ at the transition and in the vicinity of T_0 , α_2 may be written as a linear function of temperature:

$$\alpha_2(T) = \tilde{\alpha}_2(T - T_0), \quad (2.5)$$

where $\tilde{\alpha}_2$ is a positive constant.

If we restrain our consideration to the case where the two possibilities of broken symmetry for ψ and $-\psi$ are equivalent, even power terms are the only ones that survive in the free energy expansion. Generally, the $\alpha_{n \geq 4}$ parameters are only weakly temperature dependent and may be taken as a positive constant. Thus the order after which the series may be truncated depends on the first positive $\alpha_{n \geq 4}$ coefficient, as subsequent terms cannot alter the critical behavior of the system. More precisely, it can be shown that second and first order thermodynamic phase transitions are adequately described by truncating the expansion after the fourth and sixth order, respectively. For a second-order phase transition, Eq. (2.3) therefore reads:

$$F = F_0 + \frac{1}{2} \tilde{\alpha}_2 (T - T_0) \psi^2 + \frac{1}{4} \alpha_4 \psi^4, \quad (2.6)$$

³ The order parameter may be a scalar, a vector, a complex number, or a more complicated quantity. For the purpose of simplicity, we will take it to be a scalar in the present demonstration.

⁴ Landau's theory considers the Helmholtz free energy F ; instead, one can also expand the Gibbs free energy $G(p, T, \psi)$ to get pressure- and temperature-dependent coefficients.

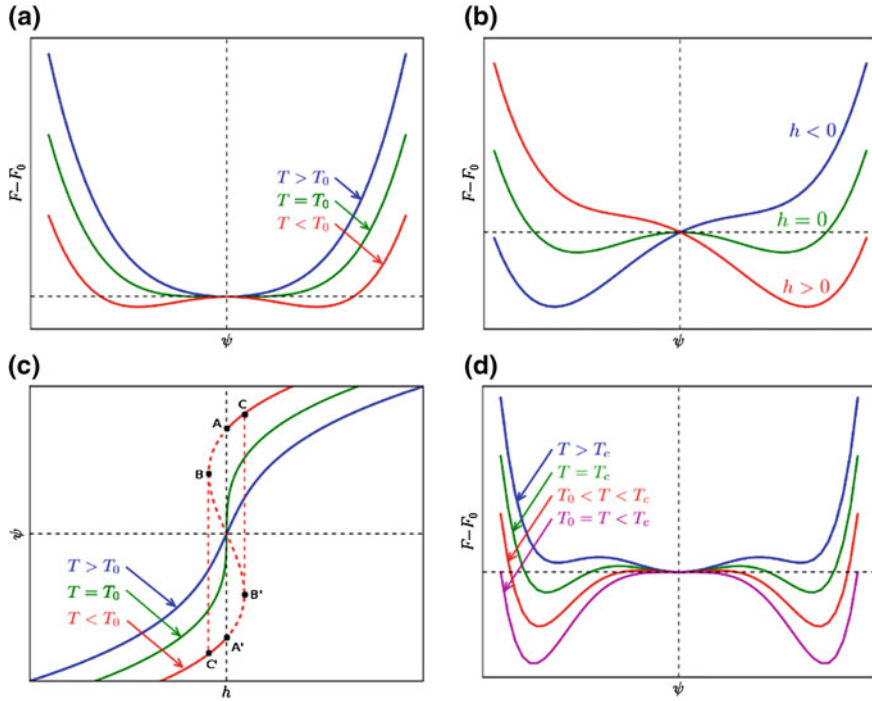


Fig. 2.3 Thermodynamic phase transitions described by Landau-Ginzburg-Devonshire theory. **a** Free energy versus order parameter in the vicinity of a second-order phase transition, with T_0 the Curie-Weiss temperature. **b** Asymmetry of the double-well configuration in presence of an external field. **c** Evolution of the order parameter with the external field; for $T < T_0$, a hysteresis appears. **d** Free energy versus order parameter in the vicinity of a first-order phase transition, showing the intermediate regime given by the critical temperature T_c where three minima coexist at $F = 0$

with $\alpha_4 > 0$, and the stability condition is given by:

$$\partial F / \partial \psi = 0 = \tilde{\alpha}_2(T - T_0)\psi + \alpha_4\psi^3. \quad (2.7)$$

In the high symmetry phase (i.e. for $T > T_0$), the quadratic term in Eq. (2.7) is positive, meaning that the only minimum is at $\psi = 0$. For $T < T_0$, the extrema of the function are $\psi = 0$ and $\psi = \pm (\alpha_2/\alpha_4)^{1/2} (T_0 - T)^{1/2}$, where only the latter two are minima. As can be seen in Fig. 2.3a, this corresponds to the existence, below the transition temperature T_0 , of two energy-equivalent stable states, yielding the so-called *double-well potential*. The transition can be identified as second order, since ψ goes continuously to zero as T approaches T_0 , and T_0 with the Curie-Weiss temperature.

It is easy, from Eq. (2.6), to consider the effect of an external field h on the free energy, which may be added as a simple linearly coupled term:

$$F = F_0 + \frac{1}{2}\tilde{\alpha}_2(T - T_0)\psi^2 + \frac{1}{4}\alpha_4\psi^4 - h\psi. \quad (2.8)$$

In the cases where $h \neq 0$, the free energy becomes asymmetric about ψ : above T_0 , the free energy minimum is not at $\psi = 0$, and below T_0 the two minima are not equal anymore. The latter case is illustrated in Fig. 2.3b, for $h < 0$ and $h > 0$. From the stability condition, we obtain the equation of state:

$$\partial F / \partial \psi = 0 = \tilde{\alpha}_2(T - T_0)\psi + \alpha_4\psi^3 - h, \quad (2.9)$$

which can be used to monitor the evolution of ψ as a function of the applied field. In the representation shown in Fig. 2.3c for $T < T_0$, the solid lines refer to stable and the dashed lines to unstable states of the system. The segments $A-B$ and $A'-B'$ correspond to metastable states, while the segments $B-O$ and $B'-O'$ refer to unstable states with $\partial^2 F / \partial h^2 < 0$. Therefore, when h is varied, ψ and F exhibit discontinuities between the states corresponding to the points $B-C'$ and $C-B'$, yielding the well-known *hysteresis loop* $C-A-B-C'-A'-B'$, with a coercive field equal to $(h_{B'} - h_B)/2$.

First-order phase transitions may be treated in a similar fashion, with the free energy expansion given this time by:

$$F = F_0 + \frac{1}{2}\tilde{\alpha}_2(T - T_0)\psi^2 + \frac{1}{4}\alpha_4\psi^4 + \frac{1}{6}\alpha_6\psi^6, \quad (2.10)$$

where $\alpha_4 < 0$ and $\alpha_6 > 0$. Here, the transition between a high temperature phase with a single energy minimum at $\psi = 0$ and a low temperature phase with two nonzero equivalent ground states is marked by the intermediate onset of three equivalent minima at $F = 0$, thus defining a critical temperature T_c :

$$\begin{aligned} F - F_0 = 0 &= \frac{1}{2}\tilde{\alpha}_2(T - T_0)\psi^2 - \frac{1}{4}|\alpha_4|\psi^4 + \frac{1}{6}\alpha_6\psi^6, \\ \partial F / \partial \psi = 0 &= \tilde{\alpha}_2(T - T_0)\psi - |\alpha_4|\psi^3 + \alpha_6\psi^5. \end{aligned} \quad (2.11)$$

Solving for $T = T_c$ and $\psi \neq 0$, we obtain:

$$T_c = T_0 + \frac{3}{16} \frac{\alpha_4^2}{\tilde{\alpha}_2\alpha_6} \quad (2.12)$$

where we see that $T_c > T_0$. As can be seen in Fig. 2.3d, three stable states therefore exist for $T_c \geq T > T_0$, and the double-well configuration is recovered for $T \leq T_0$.

As a thermodynamic formalism purely based on the intrinsic symmetries of the system, LGD theory offers a simple and elegant way to understand the basic definition of an ideal ferroic material. Below the Curie-Weiss temperature, two or more equivalent ground states correspond to finite (opposite) values of the adequate order parameter, and the application of an external field results in the asymmetrization of the double-well potential, thus allowing reversible switching between the ground states and the appearance of the characteristic hysteresis loop. In practice, three


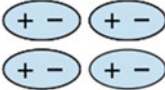
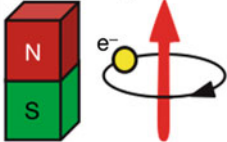
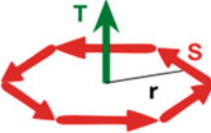
<div>Space</div> <div>Time</div>	Invariant	Change
Invariant	<div>Ferroelastic</div> 	<div>Ferroelectric</div> 
Change	<div>Ferromagnetic</div> 	<div>Ferrotoroidic</div> 

Fig. 2.4 The four ferroic orders, classified under the parity operations of space and time. Reprinted from [7]

categories of ferroic materials are well known and characterized: ferromagnetic materials possess a spontaneous magnetization, reversible under a magnetic field; ferroelectrics possess a spontaneous electric polarization, reversible under an electric field; and ferroelastic material possess a spontaneous deformation, reversible under an applied strain. From considerations of parity operations under space and time reversal, a fourth ferroic order, ferrotoroidicity (Fig. 2.4), was originally theoretically suggested, and recently observed [7]. These different ferroic orders can coexist and may couple, in materials known as multiferroics. Driven by the needs of memory applications, where electrically switchable, magnetically readable elements would greatly improve energy efficiency, much recent research has focused specifically on magnetoelectric multiferroics [8, 9].

2.3 Microscopic Origin of Ferroelectricity

From the first discovery of ferroelectricity in 1920 [5] and for almost three decades afterwards, all known ferroelectric compounds presented a hydrogen bonded structure. A turning point was reached in 1949 with the discovery of ferroelectricity in BaTiO_3 , whose much simpler crystal structure spurred scientific progress towards understanding the physics of ferroelectricity on the microscopic scale. BaTiO_3 was the first recognized ferroelectric member of one of the most intensively studied families of transition metal oxides, the *perovskite* oxides family. Named after the eponymous (nonferroelectric) CaTiO_3 , perovskite oxides share a common crystal

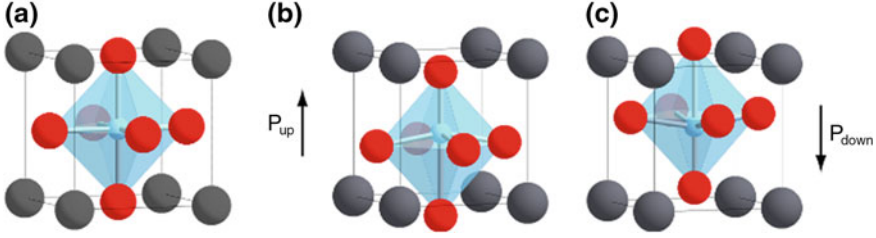


Fig. 2.5 Unit cell of the perovskite structure of PbTiO_3 in the (a) paraelectric cubic phase and (b, c) tetragonal ferroelectric phase. In the latter, the off-centering of the central (B) cation and the oxygen octahedron along the polar z axis give rise to an electric dipole at the origin of the ferroelectric polarization. The energy-equivalent states corresponding to an off-centering towards $z+$ and $z-$ are usually referred to as “up” and “down” polarization. Original images by Dr. N. Stucki

structure derived from the ideal cubic perovskite. Their general chemical formula is ABO_3 , where A is a mono-, di- or tri-valent A cation and B a tri-, tetra- or penta-valent cation, respectively. In the centrosymmetric cubic structure, the A cations are located the corners of the unit cell, the B cation are body-centered, and the oxygen anions are face-centered, as illustrated in Fig. 2.5a.

At the origin of the multiple possible functionalities of perovskite oxides, different instabilities may arise that distort the crystal structure from the ideal cubic symmetry. The likelihood of symmetry-lowering distortions can be phenomenologically understood by considering the size of the A and B cations, and is often quantified through the Goldschmidt tolerance factor:

$$t = \frac{R_A + R_O}{\sqrt{2}R_B + R_O}, \quad (2.13)$$

where R_A , R_B , and R_O are the ionic radii of the A, B, and O atoms. In the case where $t = 1$, the structure is frozen in the cubic phase, which corresponds to the ions having no free space to move. For $t > 1$, the B cation is free to move off-center, thus generating an electric dipole, and the material is termed B-site driven. A-site driven materials with $t < 1$ are often not ferroelectric, as the larger B cation favors the rotation of the oxygen octahedra. Many perovskite ferroelectrics, such as BaTiO_3 , present a B-site driven displacive ferroelectric polarization, with the cooperative alignment of the dipoles of neighboring unit cells. One notable exception is PbTiO_3 , the base material structure studied in the present thesis, where the hybridization between the Pb^{2+} A cations and the O^{2-} anions leads to a large strain, stabilizing a tetragonal structure, and induces hybridization between the Ti^{4+} B cation and the oxygens, allowing the off-centering of the Ti with respect to the oxygen octahedron. Moreover, the Ti atom and oxygen octahedron are both displaced in the same direction with respect to the Pb, thus yielding a finite electric dipole. Figure 2.5b, c illustrates this particular case, where the two energy-equivalent possible atomic displacements lead to either “up” or “down” polarization.

More quantitatively, the instability at the origin of ferroelectricity in the perovskite structure has been associated with the existence of a “soft mode” in the phonon band structure of the cubic symmetry. A transverse phonon mode is said to soften when the ionic displacements associated with its eigenmodes lead to a decrease in energy of the system. Thus in this case the atoms are subjected to a driving force that distorts the crystal structure into a lower symmetry, stable ground state. The phonon mode dispersion can be calculated from first principles, allowing ferroelectric instabilities to be identified as imaginary frequencies of modes at the center of the cubic Brillouin zone [10]. According to the classical model established by C. Cochran in 1960, the stabilization of the polar distortion relies on the competition between short range forces between the B cation and its nearest neighbors and the long range Coulomb (dipole-dipole) interaction throughout the material. In the simplest picture, these competing interactions contribute to the frequency of the transverse optical phonon, and the cancellation of both terms can lead to a structural instability. However, understanding of the specific microscopic mechanism of a given material also requires the nature of the bonding between the ions to be taken into account. In particular, as described previously, the covalent nature of the Pb-O bond in PbTiO_3 plays a significant role in the ferroelectric instability, in contrast with the primary contribution of the Ti and apical O atomic chains in BaTiO_3 . In first principles approaches, these material-specific properties can be quantified via the Born effective charge, which measures the linear contribution of a lattice distortion to the polarization.

2.4 Domain Formation in Ferroelectric Thin Films

The growth of ferroelectric samples in the form of epitaxial thin films present numerous advantages from an applied perspective. Following the steady refinements of different deposition techniques, many ferroelectric perovskites can nowadays be routinely grown with single-crystal quality, with a precise control of the film thickness up to an atomic layer. Moreover, the choice of atomically smooth, high quality, crystalline substrate allows the in-plane parameters of the film to be constrained, which has been shown to prove critical for the functionalities linked to the crystal structure [11, 12]. In a large part of the research on oxide thin films, sputtering and pulsed laser deposition (PLD) were used. In both techniques, components of the desired material are ejected from a stoichiometric source target (usually in ceramic form) onto the substrate. In sputtering, a plasma is created by the application of a high voltage between the target and the substrate, which bombards the target and ejects atoms. A magnetic field created by permanent magnets behind the target confines the plasma, and increases the sputtering rate. As ejected particles reach the substrate, charges build up on the surface if the deposited material is insulating. For this reason, alternating radio-frequency voltages are used. In the case of PLD, particles are ejected from the target using a high energy laser beam, and transferred onto the substrate in gaseous form. As no magnetic fields are involved in PLD, the growth of the film may be controlled in situ by the use of reflection high-energy electron

diffraction (RHEED), which allows real-time monitoring of the film thickness and growth mode.

From basic electrostatics, bound charges arise at the surface of a polarized dielectric material following

$$\rho_b = -\nabla \cdot \mathbf{P}, \quad (2.14)$$

where ρ_b is the volume bound charge density. In ferroelectric materials, bound charges therefore lead to the existence of an internal electric field opposite to the spontaneous polarization. As the dimensions of the sample are reduced, this so-called depolarizing field can become strong enough to completely suppress the polarization. For this reason, if the depolarizing field is not screened, ferroelectricity disappears below a critical film thickness initially thought to be relatively large (of the order of 100 nm) [14], although later experiments demonstrated that the ferroelectric state could be maintained in ultrathin films down to a few monolayer [15–17]. In the simplest cases, a reduction of the depolarizing field can arise with the presence of screening charges at the sample surface, such as chemical adsorbates (most often water molecules) from the surrounding environment. The screening efficiency of molecular adsorbates was particularly demonstrated by Wang et al., who achieved polarization reversal in PbTiO_3 thin films by varying the partial oxygen pressure of a controlled environment [18]. Figure 2.6, reprinted from [13], reviews the different mechanisms that can arise to compensate for the depolarizing field in thin films. Aside from molecular adsorbates from the environment, the buildup of screening charges can be obtained if the sample is mounted in a capacitor geometry between two metallic electrodes, or, in extreme cases, from mobile charges from within the semiconducting material itself.

In absence of sufficient screening charges, the accumulation of bound charges can be avoided through the formation of periodic ferroelectric domains of alternating polarization [20]. In this case, the bound surface charge vanishes on average and the magnitude of the local depolarizing fields within the ferroelectric thin film is greatly decreased. However, stray fields originating from the formation of domain walls significantly contribute to the total energy of the system, and the configuration of the polydomain state therefore depends on the depolarizing fields of the original unscreened system. This problem was tackled by C. Kittel for ferromagnetic thin films [19], as shown in Fig. 2.7. In this study, three possible states were considered for the magnetization, corresponding to an out-of-plane polydomain structure, with (I) or without (II) flux-closure magnetization rotation (so-called “Landau-Lifshitz domains”) near the film top and bottom surfaces, or a purely monodomain in-plane magnetization (III). As shown by calculations of the total energy as a function of the film thickness, (III) is the energetically most favorable configuration for ultrathin films, followed by a transition to (I) for intermediate thickness and finally (II) for thicker films. In ferromagnetic materials, where the magnetization is related to the ordering of microscopic spins, and no monopoles exist, the type of domain structure is defined by the energy balance between the energy cost of divergent or unclosed field lines originating from the magnetic structure, and the energy cost of the domain wall. For a periodic, out-of-plane domain structure, the balance between these two

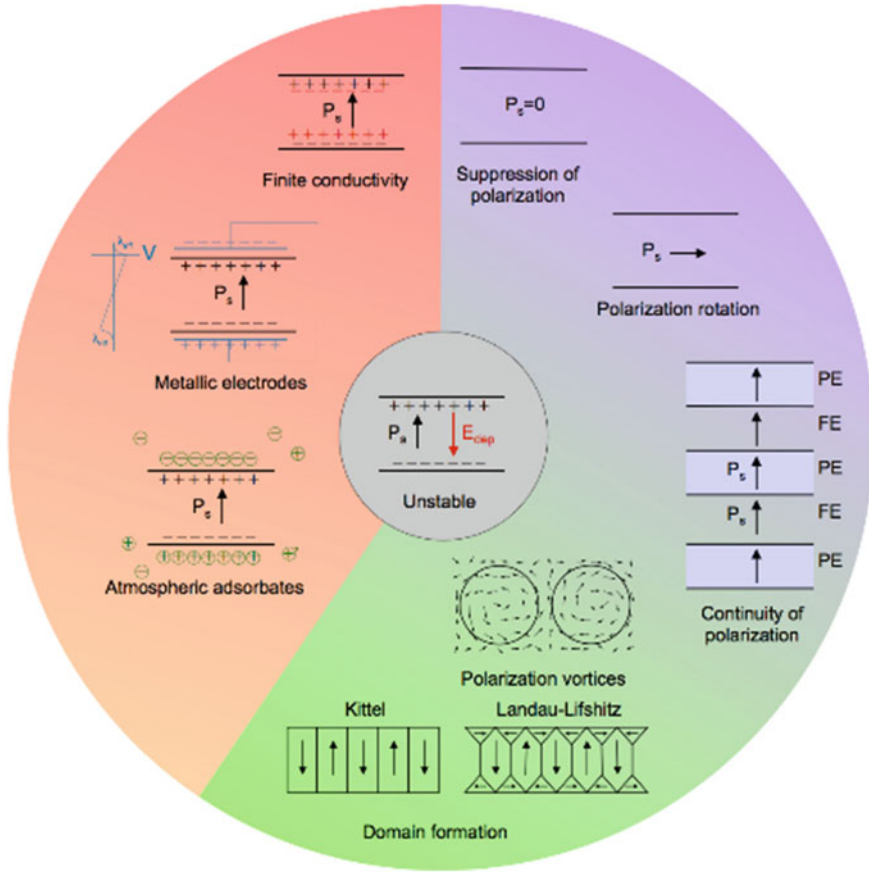


Fig. 2.6 Effects of the depolarizing field in ferroelectric thin films, reprinted from [13]. *The left side of the diagram illustrates different mechanisms for screening of the surface bound charges, allowing the ferroelectric state to be uniformly maintained throughout the sample. If the screening is insufficient, the ferroelectric state can be preserved through the formation of domains or rotation of the polarization vector, as shown on the right side of the diagram. If all else fails, the polarization is suppressed*

terms will determine the period width, obeying the Landau-Lifshitz-Kittel scaling relation:

$$w = \sqrt{\frac{\sigma}{U}}d, \quad (2.15)$$

where w is the period of the domain structure, d the thickness of the film, U the volume energy density of the domain and σ the energy density per unit area of the domain wall. In ferroelectric materials, this relation was found to be valid over a remarkable wide range of thicknesses, providing the polarization is unscreened or only weakly screened [21]. However, the fundamentally different physical origins of

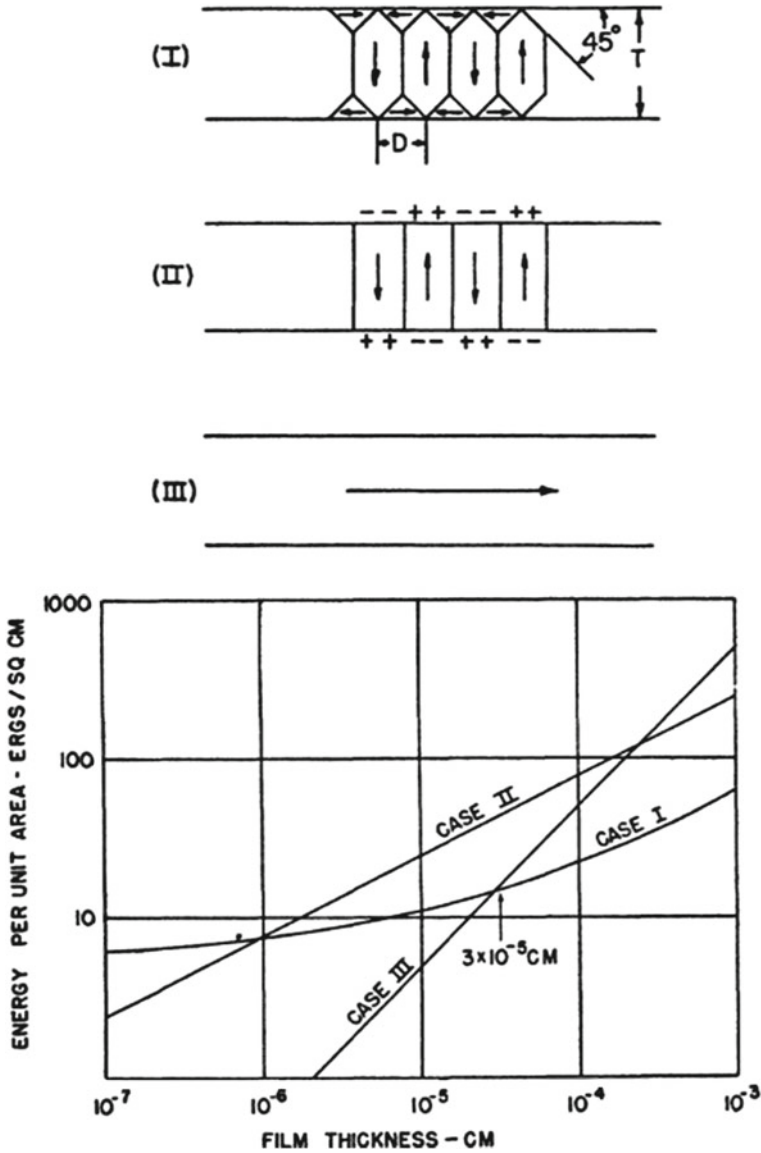
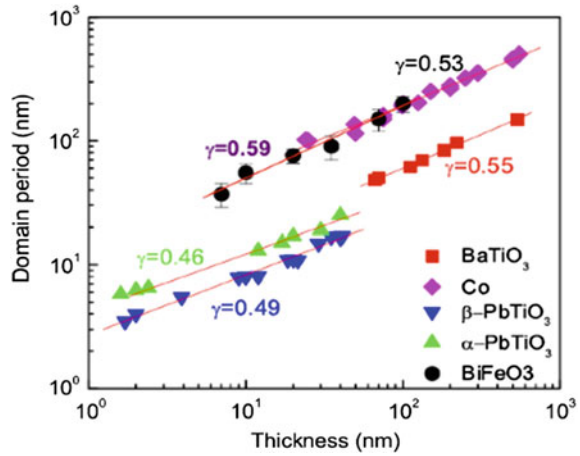


Fig. 2.7 Energy of different domain wall configurations in ferromagnetic thin films as function of film thickness, as analyzed by C. Kittel in [19]. For ultrathin films, the lowest energy is obtained for a monodomain in-plane configuration (III), while a periodic arrangement of out-of-plane domains is more favorable for thicker films. In between these extremes the most stable configuration corresponds to Landau-Lifshitz domains, characterized by flux-closure rotation of the magnetization near the top and bottom interfaces

Fig. 2.8 Landau-Lifshitz-Kittel scaling for different ferroic materials, showing the clearly smaller domain periodicity in ferroelectric materials with respect to ferromagnets. Interestingly, the antiferromagnetic-ferroelectric (multiferroic) BiFeO_3 follows the trend of ferromagnetic Co, suggesting intricate mechanisms when two or more ferroic orders are combined. Reprinted from [21]



ferromagnetism and ferroelectrics still lead to significant differences between domain structures in these two types of materials. As shown by studies of domain periodicity in various ferroic materials, shown in Fig. 2.8, at comparable film thicknesses significantly narrower domains are encountered in ferroelectric with respect to ferromagnetic thin films [22]. In ferroelectrics, screening of the surface bound charges set by the electrical boundary conditions therefore interfere with the Landau-Lifshitz-Kittel law and play an active part in the formation of a monodomain or polydomain state. But perhaps more importantly, the structural nature of the interface between two domains, referred to as a *domain wall*, differs also significantly between ferromagnetic and ferroelectric materials.

2.5 Structural Properties of Ferroelectric Domain Walls

In ferromagnets, the typical energy of a domain wall is primarily governed by exchange, which favors parallel alignment of the spins, and magnetic domain walls therefore usually exhibit a gradual rotation of spins over lengths of the order of tens to hundreds of nanometers, leading to so-called Bloch or Néel type domain walls. In ferroelectrics, the domain wall energy is rather dominated by the very strong coupling between the polarization and the strain, and polarization reversal therefore occurs on a much shorter scale of a few unit cells. To a good approximation, 180° ferroelectric domain walls in perovskite ferroelectrics with out-of-plane polarization can therefore be considered Ising-like, i.e. with no in-plane component associated with polarization rotation. Thus, while the flux-closure of Landau-Lifshitz domain pattern shown in Fig. 2.7(I) was observed for a long time in ferromagnets, it was originally thought unlikely to form in ferroelectrics due to the very large crystalline anisotropy that makes polarization rotation difficult. However, closure domains were

recently demonstrated to potentially play a significant role in domain stabilization in first principles calculations of ultrathin ferroelectric capacitors [24]. In similar studies, Lee et al. associated this small in-plane rotation with a mixed Bloch-Néel-Ising character of the domain walls [23], as illustrated in Fig. 2.9. In both approaches, the domain wall remains of unit-cell thickness and predominantly Ising-like character, but is suggested to possess an intrinsic structure more complex than initially proposed [25].

More recently, these theoretical suggestions were experimentally confirmed with the refinement of high resolution transmission electron microscopy (HRTEM), allowing the observation of domain walls at the atomic scale [26]. In a study using HRTEM to probe the atomic structure of 180° domain walls in tetragonal perovskite $\text{Pb}(\text{Zr}_{0.2}\text{Ti}_{0.8})\text{O}_3$ (a solid solution with structural and electronic properties close to PbTiO_3), Jia et al. revealed the domain wall configuration to be in fair agreement with the theoretical predictions. A sample measurement is shown in Fig. 2.10. As can be seen in this image, the polarization reversal occurs over a few unit cells, and a small decrease of the out-of-plane (z -axis) polarization can be seen on either side of the wall, thus confirming the Ising-like character. Near the bottom electrode, consisting of a very thin 2.5 unit cell metallic SrRuO_3 layer (therefore providing only weak screening of the bound charges), a polarization rotation can be observed, in order to stabilize the domain wall through the formation of a closure domain. A final, very interesting observation, that goes beyond simple theoretical models, concerns the presence of steps along the length of the domain wall, with a width of one or two unit cells. At these steps, the microscopic dipole moments of neighboring unit cells are anti-aligned, an energetically highly unfavorable configuration which could, by itself, not remain stable. In order for this configuration to be stable, the polarization discontinuities must be screened by the presence of charged defects, such as the ubiquitous oxygen vacancies in such films.

Fundamentally, ferroelectric domain walls can therefore be seen as topological defects in the parent crystal structure of the material, showing local variations in symmetry and strain. Due to their extremely small width, they moreover form structural interfaces of intrinsically nanometer scale dimensions. However, as already suggested by the previous report of step features in domain walls, the formation and structure of domain walls in ferroelectric thin films cannot be understood from the sole point of view of depolarizing field and screening charges. In real samples, defects in the crystal structure play a governing role. On the one hand, mobile (usually point-like) defects may be localized at domain walls, accommodating the locally different symmetry; on the other hand, domain walls can become pinned by defects, thus minimizing their potential energy. Domain wall pinning was demonstrated in first principle studies for PbTiO_3 [27], and is generally regarded as a crucial parameter in the domain wall motion occurring during domain growth events. In that respect, many different approaches were considered to link the domain wall mobility to the material-specific defect types and densities, one of which forms the focus of Chaps. 6–8 of this thesis.

Perhaps the most striking feature of ferroelectric domain walls, a take-home message serving as a lead-in for the rest of this manuscript, is the existence of

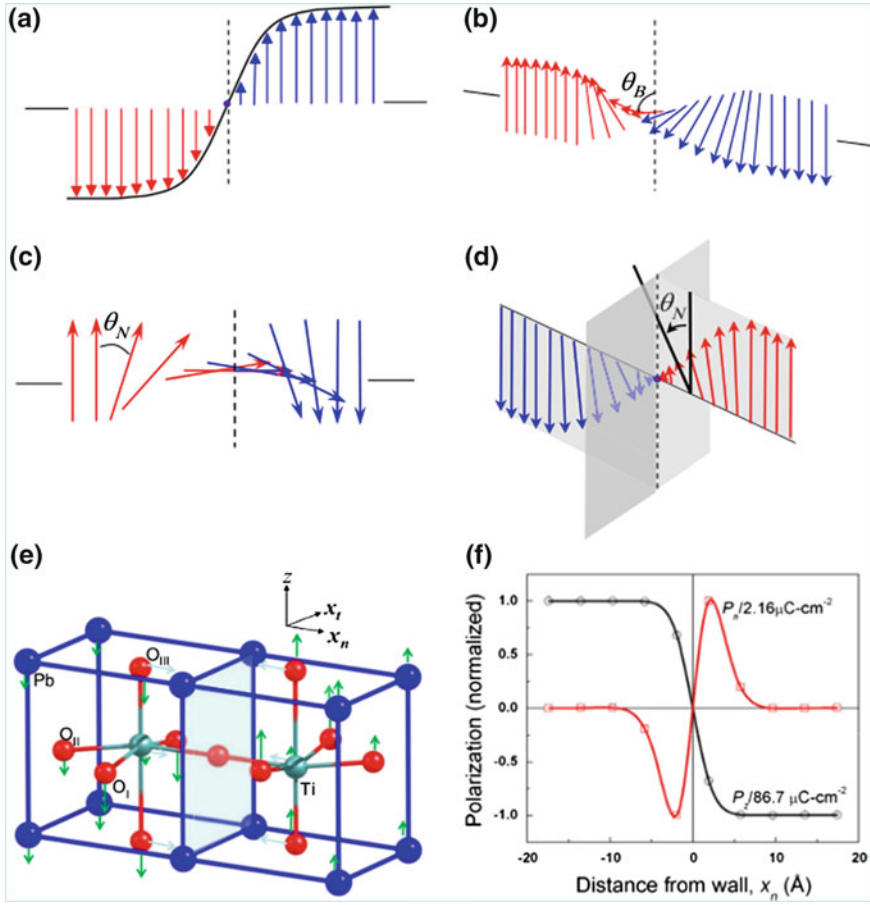


Fig. 2.9 Different types of ferroic domain walls. **a** Ising type, showing a gradual magnitude variation but no rotation of the order parameter. **b** Bloch type, showing a gradual rotation with angle θ_B out-of-plane with respect to the order parameter, and no change in magnitude. **c** Néel type, showing an in-plane rotation with angle θ_N and no change in magnitude. **d** Mixed Ising-Néel type, showing both in-plane rotation and decrease of the magnitude. A mixed Ising-Bloch type would be similar, with an out-of-plane rotation. **e** Atomic displacements in the unit cells forming a ferroelectric domain wall, calculated from first principles. The normalized polarization (**f**) reveals a finite in-plane component (red curve) associated with the reversal of the out-of-plane component (black curve), thus suggesting the mixed character of ferroelectric domain walls. Reprinted from [23]

local functionalities, absent from the bulk parent material but arising on these very small scales due to the changes in topology and defect concentration. For instance, as will be shown in Chap. 4, the locally broken symmetry due to the change in polarization has significant consequences on the piezoelectric properties. Also, a lot of attention was recently focused on the transport properties: in an original study on the antiferromagnetic-ferroelectric BiFeO₃, Seidel et al. showed that domain

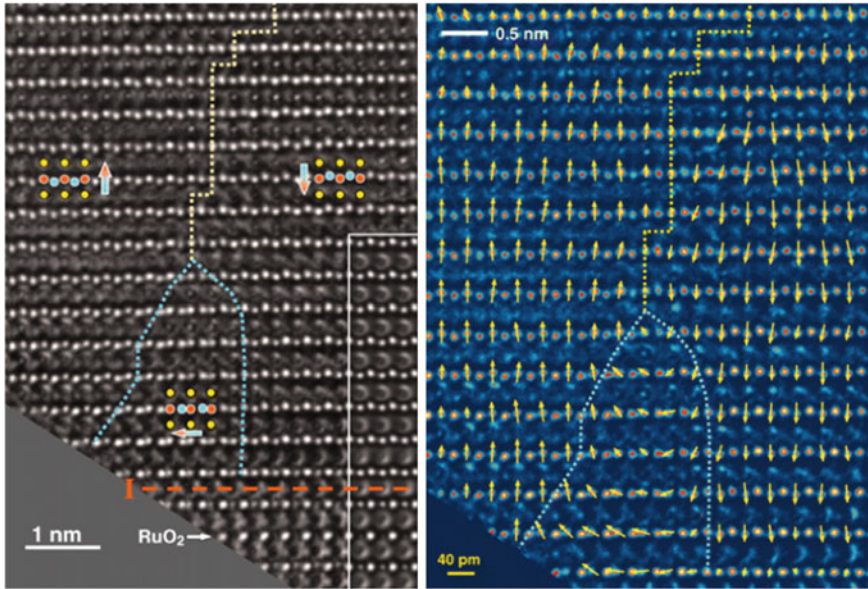


Fig. 2.10 HRTEM image of a 180° domain wall in a tetragonal perovskite $\text{Pb}(\text{Zr}_{0.2}\text{Ti}_{0.8})\text{O}_3$ thin film, with a bottom metallic layer of SrRuO_3 (marked by the horizontal dashed line). On the right side, the atomic displacement vectors are showed in order to help visualize the polarization rotation near the bottom interface. Another notable feature is the domain wall steps visible in the upper part, suggesting the presence of charged defects to stabilize this energy unfavorable configuration. Reprinted from [26]

walls behaved as conductive channels within an otherwise dielectric material [28]; subsequently, these same domain walls were suggested to exhibit photovoltaic properties as well [29]. The former effect, studied in a simpler tetragonal perovskite ferroelectric, will be discussed in Chap. 5. More generally, a range of increasingly varied functionalities was and is being reported in ferroic domain walls. Notable examples include the possible polar nature of ferroelastic domain walls in SrTiO_3 , either intrinsically due to local gradient coupling or extrinsically through defect accumulation [30], or magnetic ordering in ferroelectric domain walls [31].

References

1. B. Jaffe, W.R. Cook, H. Jaffe, *Piezoelectric Ceramics* (R. A. N, Ohio, USA, 2002)
2. Veeco Instruments Inc. (2008) *Piezoresponse Atomic Force Microscopy Using a Nanoscope V Controller*
3. D. Brewster, Observations of the pyro-electricity of minerals. *Edinb. J. Sci.* **1**, 208 (1824)
4. J. Curie, P. Curie, Development, via compression, of electric polarization in hemihedral crystals with inclined faces. *Bull. Soc. minéral. Fr.* **3**, 90 (1880)
5. J. Valasek, Piezo-electric and allied phenomena in rochelle salt. *Phys. Rev.* **17**, 475 (1921)

6. J.M. Yeomans, *Statistical Mechanics of Phase Transitions* (Oxford University Press, New York, 2002)
7. B.B. Van Aken, J.-P. Rivera, H. Schmid, M. Fiebig, Observation of ferrotoroidic domains. *Nature* **449**, 702 (2007)
8. W. Eerenstein, N.D. Mathur, J.F. Scott, Multiferroic and magnetoelectric materials. *Nature* **442**, 759 (2006)
9. J.F. Scott, Electrical characterization of magnetoelectrical materials. *J. Mat. Res.* **22**, 2053 (2007)
10. P. Ghosez, E. Cockayne, U.V. Waghmare, K.M. Rabe, Lattice dynamics of BaTiO_3 , PbTiO_3 , and PbZrO_3 : a comparative first-principles study. *Phys. Rev. B* **60**, 836 (1999)
11. K.H. Ahn, T. Lookman, A.R. Bishop, Strain-induced metal-insulator phase coexistence in perovskite manganites. *Nature* **428**, 401 (2004)
12. G. Catalan, A. Janssens, G. Rispens, S. Csiszar, O. Seeck, G. Rijnders, D.H.A. Blank, B. Noheda, Polar domains in lead titanate films under tensile strain. *Phys. Rev. Lett.* **96**, 127602 (2006)
13. C. Lichtensteiger, P. Zubko, M. Stengel, P. Aguado-Puente, J.-M. Triscone, P. Ghosez, and J. Junquera, *Oxide Ultrathin Films: Science and Technology*, chapter 12. (Wiley, Weinheim 2012)
14. M.E. Lines, A.M. Glass, *Principles and Applications of Ferroelectrics and Related Materials* (Oxford University Press, Oxford, 1977)
15. A.V. Bune, V.M. Fridkin, S. Ducharme, L.M. Blinov, S.P. Palto, A.V. Sorokin, S.G. Yudin, A. Zlatkin, Two-dimensional ferroelectric films. *Nature* **391**, 874 (1998)
16. T. Tybell, C.H. Ahn, J.-M. Triscone, Ferroelectricity in thin perovskite films. *Appl. Phys. Lett.* **75**, 856 (1999)
17. J. Junquera, P. Ghosez, Critical thickness for ferroelectricity in perovskite ultrathin films. *Nature* **422**, 506 (2003)
18. R.V. Wang, D.D. Fong, F. Jiang, M.J. Highland, P.H. Fuoss, C. Thompson, A.M. Kolpak, J.A. Eastman, S.K. Streiffer, A.M. Rappe, G.B. Stephenson, Reversible chemical switching of a ferroelectric film. *Phys. Rev. Lett.* **102**, 047601 (2009)
19. C. Kittel, Theory of the structure of ferromagnetic domains in films and small particles. *Phys. Rev.* **70**, 965 (1946)
20. C. Lichtensteiger, M. Dawber, N. Stucki, J.-M. Triscone, J. Hoffman, J.-B. Yau, C.H. Ahn, L. Despont, P. Aebi, Monodomain to polydomain transition in ferroelectric PbTiO_3 thin films with $\text{La}_{0.67}\text{Sr}_{0.33}\text{MnO}_3$ electrodes. *Appl. Phys. Lett.* **90**, 052907 (2007)
21. G. Catalan, J.F. Scott, A. Schilling, J.M. Gregg, Wall thickness dependence of the scaling law for ferroic stripe domains. *J. Phys.: Condens. Matter* **19**, 022201 (2007)
22. G. Catalan, H. Béa, S. Fusil, M. Bibes, P. Paruch, A. Barthélémy, J.F. Scott, Fractal dimension and size scaling of domains in thin films of multiferroic BiFeO_3 . *Phys. Rev. Lett.* **100**, 027602 (2008)
23. D. Lee, R.K. Behera, P. Wu, H. Xu, Y.L. Li, S.B. Sinnott, W.R. Phillpot, L.Q. Chen, V. Gopalan, Mixed bloch-Néel-ising character of 180° ferroelectric domain walls. *Phys. Rev. B* **80**, 060102 (2009)
24. P. Aguado-Puente, J. Junquera, Ferromagneticlike closure domains in ferroelectric ultrathin films: first-principles simulations. *Phys. Rev. Lett.* **100**, 177601 (2008)
25. B. Meyer, D. Vanderbilt, Ab initio study of ferroelectric domain walls in PbTiO_3 . *Phys. Rev. B* **65**, 104111 (2002)
26. C.-L. Jia, K.W. Urban, M. Alexe, D. Hesse, I. Vrejoiu, Direct observation of continuous electric dipole rotation in flux-closure domains in ferroelectric $\text{Pb}(\text{Zr}, \text{Ti})\text{O}_3$. *Science* **331**, 1420 (2011)
27. L. He, D. Vanderbilt, First-principles study of oxygen-vacancy pinning of domain walls in PbTiO_3 . *Phys. Rev. B* **68**, 134103 (2003)
28. J. Seidel, L.W. Martin, Q. He, Q. Zhan, Y.-H. Chu, A. Rother, M.E. Hawkrige, P. Maksymovych, P. Yu, M. Gajek, N. Balke, S.V. Kalinin, S. Gemming, F. Want, G. Catalan, J.F. Scott, N.A. Spaldin, J. Orenstein, R. Ramesh, Conduction at domain walls in oxide multiferroics. *Nature Mater.* **8**, 229 (2009)

29. S.Y. Yang, J. Seidel, S.J. Byrnes, P. Shafer, C.-H. Yang, M.D. Rossell, P. Yu, Y.-H. Chu, J.F. Scott, J.W. Ager III, L.W. Martin, R. Ramesh, Above-bandgap voltages from ferroelectric photovoltaic devices. *Nature Nanotech.* **5**, 143 (2010)
30. P. Zubko, G. Catalan, A. Buckley, P.R.L. Welche, J.F. Scott, Strain-gradient-induced polarization in SrTiO_3 single crystals. *Phy. Rev. Lett.* **99**, 167601 (2007)
31. J. Privratska, V. Janovec, Spontaneous polarization and or magnetization in non-ferroelastic domain walls: symmetry predictions. *Ferroelectrics* **222**, 23 (1999)

Ferroelectric Domain Walls

Statics, Dynamics, and Functionalities Revealed by
Atomic Force Microscopy

Guyonnet, J.

2014, XV, 159 p. 96 illus., 17 illus. in color., Hardcover

ISBN: 978-3-319-05749-1